Green Synthesis Of Bimetallic Iron/Copper Nanoparticles Using Ficus Leaves Extract For Removing Orange G(OG) Dye From Aqueous Medium

Mohammed A. Atiya*, Ahmed K. Hassan**† and Imad M. Luaibi*

*Al-Khwarizmi College of Engineering, University of Baghdad, Baghdad, Iraq
**Environment and Water Directorate, Ministry of Science and Technology, Baghdad, Iraq
†Corresponding author: Ahmed K. Hassan; emad.iq84@gmail.com

ABSTRACT

This study shows that it is possible to fabricate and characterize green bimetallic nanoparticles using eco-friendly reduction and a capping agent, which is then used for removing the orange G dye (OG) from an aqueous solution. Characterization techniques such as scanning electron microscopy (SEM), Energy Dispersive Spectroscopy (EDAX), X-Ray diffraction (XRD), and Brunauer-Emmett-Teller (BET) were applied on the resultant bimetallic nanoparticles to ensure the size, and surface area of particles nanoparticles. The results found that the removal efficiency of OG depends on the G-Fe/Cu-NPs concentration (0.5-2.0 g.L^{-1}), initial pH (2-9), OG concentration (10-50 mg.L^{-1}), and temperature (30-50 ℃). The batch experiments showed that 54% of 10 mg.L^{-1} of OG was removed within the optimum dose, pH, and temperature which were 1 g.L^{-1}, 7 and 30℃ respectively. The results of kinetic adsorption models and mechanisms indicate that OG uptake on G-Fe/Cu-NPs follows the pseudo-second-order kinetic model, physisorption, and exothermic process with (-22.9 kJ.mol^{-1}) activation energy. Adsorption isotherm investigated with models of Freundlich, Langmuir, Temkin, and Dubinin, in addition, the parameters of thermodynamic such as $\Delta G°$, $\Delta H°$, and $\Delta S°$ were -0.462 kJ.mol^{-1}, -35.88 kJ.mol^{-1}, and 0.116 kJ.mol.K^{-1} respectively, this indicted spontaneous, exothermic and favorable adsorption.

INTRODUCTION

Different wastes are generated by a variety of industries and discharged into water effluents, thereby affecting the aesthetic and quality of water and causing a serious problem by decreasing the amount of pure and clean water available in our world (Tara et al. 2019). Among these wastes are organic pollutants, especially, dyes which cause a bad effect on the environment and humans (Ismail et al. 2019).

A coloring process, which is widely employed in consumer products such as paper, plastics, textiles, cosmetics, and leather, is one of the most common industrial processes that discharge pollutants into the aqueous medium. Although dye types differ by industry, azo dyes account for more than half of all dyes used worldwide due to their versatility and chemical durability. However, discharging azo dyes into aquatic media hinders algae and other aquatic plants from absorbing sunlight and performing photosynthesis. Moreover, most azo dyes are carcinogenic in nature, toxic, and non-biodegradable, so it causes negative effects on people's health and the aquatic ecosystem (Homaeigohar 2020).

Adsorption, oxidative-reductive degradation, membrane separation, chemical coagulation, precipitation, and electro-coagulation are some of the materials and procedures that

have been utilized to clean up dye-polluted water (Atiya et al. 2020). The adsorption process, however, stands out among these approaches because of its capacity to remove organic contaminants (Campos et al. 2019).

Diverse adsorbents have been used for removing contaminants of wastewater, recently, nanotechnologies have proven to be very important in the removal of environmental pollutants, particularly, in the field of aqueous pollution. It deals with the synthesizing of tiny particles in the range of 1-100 nm which are labeled as nanoparticles (NPS). These molecules show unique properties such as small size, shape, large surface area, etc. that provide nanoparticles with better catalytic function, strong surface activity, and simple interaction with another particle (Pavithran et al. 2020).

Different techniques are used to synthesize nanomaterials such as physical technique that includes milling, vacuum sputtering, and thermal decomposition. Moreover, the chemical technique uses borohydride (NaBH$_4$) as a reduction agent. These two techniques may need a piece of sophisticated equipment, difficult conditions to control during the experiment, long procedures, and toxic capping agents. As a result, the biological method is a promising technique for overcoming these issues while achieving a safe and suitable procedure for synthesizing nanoparticles,

as well as treatment technology based on plant extract and microorganisms, which has been used as a substitute for physical and chemical techniques (Ma et al. 2020).

Due to its cost feasibility and ease of synthesis, biological synthesis utilizing plant leaf extract is a very promising technique. Plant leaves contain a considerable number of both capping and reducing agents, such as flavonoids, polyphenols, and other reducing components, which can reduce salts to zero-valent and avoid agglomeration. An abundance of plants that are free of compounds with negative side effects, non-toxic, high-efficiency, and low-cost have been certified for use in manufacturing green nanoparticles for wastewater treatment (Abd El-Aziz et al. 2020).

The ficus tree is one of the most abundant evergreens in several Asian countries and the United States. It belongs to the Moraceae family and can grow up to 30 meters in its normal habitat (Al-Qahtani 2017). Ficus contains numerous bioactive compounds such as phenolic, flavonoids, and tannins. These components are critical to the creation of ficus-zero valent iron nanoparticles (F-Fe^0) because they do not have negative or toxic side effects. They are also biodegradable, environmentally safe, and can act as capping and reducing agents.

Although iron nanoparticles (Fe-NPs) have become widely used as a promising metal in treatment processes for the removal of various environmental contaminants, however, the reactivity of (Fe-NPs) may be impacted by the development of an oxide layer around particle surfaces. To prevent this reaction, bimetal is used to protect nanoparticles from oxidizing by adding a second catalyst such as Cu, Pt, Pd, Ni to the (Fe-NPs). The mutual effect of two metals improves the properties of nanoparticles over the use of just one metal (monometallic); therefore, bimetallic nanoparticles have become of great interest to researchers. Due to the economically and safely uses of copper compared to Pd and Ni, it has been used for coating the catalyst to enhance the rate of decolorization. (Dhruval et al. 2020, Gopal et al. 2020).

This study aims to prepare different ratios of iron/copper nanoparticles using the extract from the ficus plant, then, these ratios are evaluated for selecting the effective ratio of removing orange G dye (OG) which is an example of an azo dye. Thereafter, the effective ratio is used with complete batch experiments to investigate the effects of all required experimental conditions on the OG removal.

MATERIALS AND METHODS

Chemical and Reagents

The purity of all chemicals utilized was high (99.9 %), ficus leaves were collected from the University of Baghdad at Main Campus nearest Al-Khwarizmi College, Baghdad, Iraq. The OG was purchased from Central Drug House (BDH), and Table 1 shows the properties of this dye. $FeSO_4.7H_2O$ was purchased from BDH, $CuSO_4 \cdot 5H_2O$ was purchased from Fluka, and anhydrous ethanol was purchased from Carlo Erba. The change of pH was adjusted using 1.0 M H_2SO_4 and 1.0 M NaOH solutions.

Adsorbent Preparation

The G-Fe/Cu-NPs were made using the same processes as in the previous work (AbdelAziz et al. 2019), with the following changes.

Step 1: Fresh ficus leaves were washed several times using tap water and then washed with distilled water to eliminate any impurities or dust, followed by drying in an oven at 60 °C. Additionally, they were cut using mortar and pestle into small pieces with sifting using a 2.5 mm sieve.

Step 2: The ficus leaf extract was made with 150 mL deionized water and 20 g of ficus leaf pieces, which were then boiled for 20 minutes at 70°C and then filtered to remove suspended ficus particles using filter paper. Finally, the filtrate is chilled at 4°C until it is utilized as a reducing and capping agent.

Step 3: A solution of Fe (II) and Cu (II) mixed with the ratios varying as specified for this experiment was prepared. In this study, the Fe to Cu ratio of 1:1, 3:1, and 5:1 (w/w) was chosen to determine the amount of Cu that
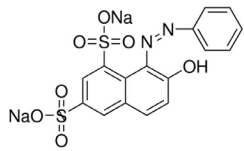
Table 1: Characteristics of OG.

Properties of OG	
Molecular structure	
Molecular formula	$C_{16}H_{10}N_2Na_2O_7S_2$
Molecular weight (g.mole^{-1})	452.37
Bulk density (kg.m^{-3})	430
Solubility in water	Soluble in water
λ_{max} (nm)	478

Table 2: The ratio between iron and copper.

Fe:Cu ratio (w:w)	Fe (g)	Cu (g)	$FeSO_4.7H_2O$ (g)	$CuSO_4 \cdot 5H_2O$ (g)
1:1	0.3	0.3	1.4935	1.1357
3:1	0.3	0.1	1.4935	0.7
5:1	0.3	0.06	1.4935	0.3929

will optimize the reactivity of the nanoparticles. The Fe: Cu ratio is made solely by measuring the weight of the two metals as shown in Table 2 below:

According to the selected ratio, $FeSO_4.7H_2O$ and $CuSO_4 \cdot 5H_2O$ salts were dissolved in 100 mL of deionized water. After the salts had completely dissolved, the impurities were removed using a filter paper filtration procedure. 100 mL of extract from step 2 was added dropwise to the 100 mL Fe (II)/Cu (II) mixture to develop the synthesis of G-Fe/Cu-NPs. The color of the mixture changed gradually from yellow to brown to black when many drops of ficus extract were added, suggesting that the metals equivalents were reduced to zero-valent and the production of G-Fe/Cu-NPs was completed. To speed up the decrease, the remaining ficus extract is added. In addition, the mixture is continually mixed for 15 minutes. The black precipitate of G-Fe/Cu-NPs nanoparticles was separated by vacuum filtration using filter paper and then washed several times with distilled water before being rinsed with 100% ethanol. The washing and rinsing processes are crucial in the synthesis because they prevent nanoparticles from oxidizing too quickly. The G-Fe/Cu-NPs were then dried at room temperature overnight before being ground to a fine powder with a mortar and pestle.

Characterization of G-Fe/Cu-NPs

To prove the chemical classification, structure, size, and surface area of nanoparticles, different techniques are used. The SEM model was used to determine the shape, topography, and average size of these nanoparticles. The EDAX approach is a confirmatory procedure that ensures each particle's identification and chemical classification. In addition, the crystallinity of the materials is examined using the XRD technique. According to the primary choices, the XRD system can precisely analyze the crystalline state of nanoparticles. Finally, the BET approach determines the specific surface area, average pore size radius, average porosity radius, and nanoparticle pore volume.

Analytical Methods

Before starting the experiments, a calibration curve for standard OG solution was done to find the maximum wavelength of dye and the equation that joined the absorbance with concentration. Thus, the maximum wavelength of OG was found to be 478 nm as shown in Fig. 1.

The ratio between the adsorbate amounts (mg) per adsorbent (g) can be defined as the adsorption capacity at equilibrium q_e and can be estimated by the following formula:

$$q_e = \frac{C_\circ - C_e}{W} \times V \qquad ...(1)$$

Where the C_o is the initial concentrations and C_e is the equilibrium concentrations of adsorbate (in $mg.L^{-1}$), V is the volume of working solution, and W is the amount of adsorbent (g).

According to the below formula the removal efficiency (RE) was calculated:

$$RE\ \% = \frac{C_o - C_t}{C_o} \times 100 \qquad ...(2)$$

Where C_t is the OG concentration at time t.

Batch Adsorption Experiments

After selecting the best ratio of Fe to Cu, characterization of nanoparticles for this ratio would be performed, and batch adsorption experiments would be carried out to evaluate the OG removal efficiency. The working solution of 50 $mg.L^{-1}$ of OG was prepared followed by adjusting pH before adding G-Fe/Cu-NPs. Some operating parameters were changed such as
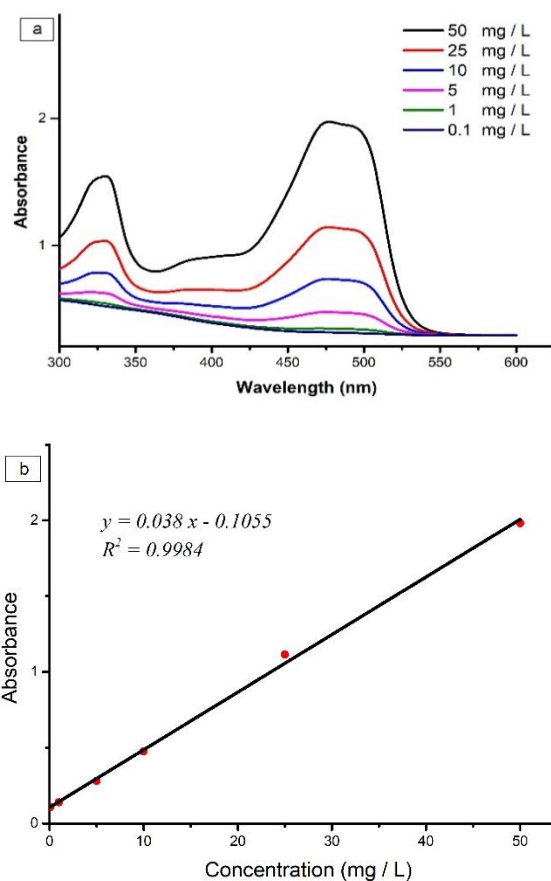
Fig. 1: UV-Vis analysis for various concentrations of OG solutions (a) Absorption and (b) Calibration plot.

G-Fe/Cu-NPs dosage ranged (0.5 – 2 g), pH ranging from (2 - 9), the range of initial OG concentrations were (10-50 mg.L^{-1}), contact time interval up to 120 min, the temperature ranged from (30 - 50 ℃), and agitation rate from (100-600 rpm). A particular amount of G-Fe/Cu-NPs was added to the OG solution and stirred using a magnetic hot plate. The temperature remained constant, and each parameter's value was tuned separately. 10 ml samples were obtained at regular intervals during each run and evaluated by UV-Vis after filtering the sample with a 0.22 μm membrane filter.

RESULTS AND DISCUSSION

Formation and Characterization of G-Fe/Cu-NPs

The change in color of the solution from yellow to brown to black indicates that the reduction process took place and that G-Fe/Cu-NPs were formed, as well as the difference in pH before and after the reduction process, with the pH of the ficus extract being 5.42 and the pH of the mixture after reduction being 3.24. As a result, the pH of the solution drops along the reduction route, moving into the more acidic range.

The G-Fe/Cu-NPs have already been characterized, and the 3:1 Fe to Cu ratio has greater removal effectiveness than the 1:1 and 5:1 ratio.

Synthesized G Fe/Cu NPs were porous and formed as semi-spherical with diameters ranging from 32 to 59 nm, as seen in SEM images in Fig. 2. The porous and hollow nanoparticles aid in the elimination of OG. Furthermore, the size fluctuation of G-Fe/Cu-NPs is owing to agglomeration caused by the magnetic nature of the NPs, as well as variations in the local concentration of the ficus extract, which is responsible for the reduction of metal ions.

The EDAX spectrum of nanoparticles presented in Fig. 3 contains further information about the synthesis of G-Fe/Cu-NPs, where the place of atomic distribution on the surface and chemical composition of G-Fe/Cu-NPs was demonstrated by the intense peaks of Fe, Cu, C, and O, 5.51 wt%, 3.33 wt%, 48.67 wt%, and 42.49 wt%, respectively. The finding of adjoint elements such as C and O signals resulted mainly from the ficus extracts that contain organic compounds C and O molecules which play a major role in the reduction and stabilizing process of G-Fe/Cu-NPs (Abd El-Aziz et al. 2020).

Fig. 4 shows the XRD curve of produced nanoparticles, which lacks any strong peaks, showing that there is no crystal structure in this case, despite a wide range of diffraction peaks (from 20o-25o). The amorphous nature of the bimetallic G-Fe/Cu-NPs generated by the green technique is demonstrated by the above result (Wang et al. 2018).

Table 3 shows the results of G-Fe/Cu-NPs surface area obtained by the BET technique. In this analysis, the pore size for G-Fe/Cu-NPs was 8.828 nm which can be classified as mesopore according to the classification of the IUPAC that categorized the pore size as macropore (50 > nm), mesopore (2 to 50 nm), super-micropore (0.7 to 2 nm) and ultra-micropore (0.7 < nm). Thus, as the catalytic performance is highly dependent on accessible pore channels due to their benefits for the diffusion of material, these size of pores provide more stability by acting as a shielding agent to prevent the harsh reaction conditions of the nanoparticles active sites (Elahimehr et al. 2020).

Best Ratio of Fe to Cu with Highest Removal Efficiency

The experiments for the three ratios are carried out, and the results show that the 3:1 ratio of Fe to Cu has the highest level of removal efficiency than the 1:1 and 5:1 ratio. As demon-
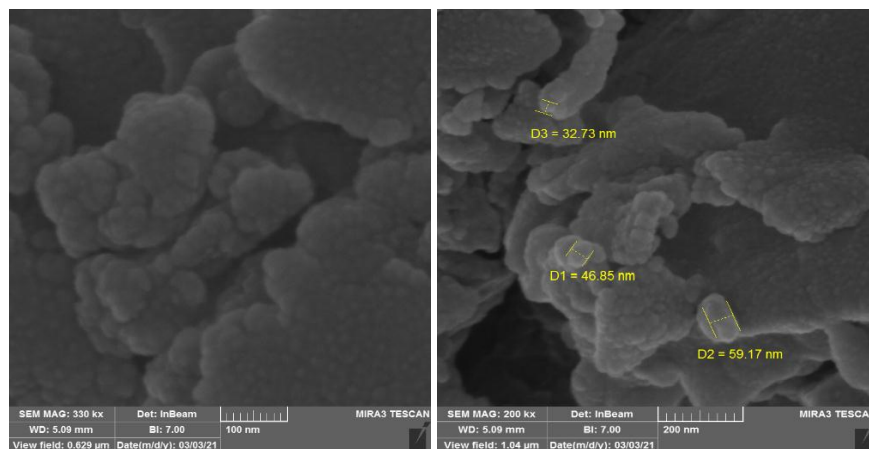

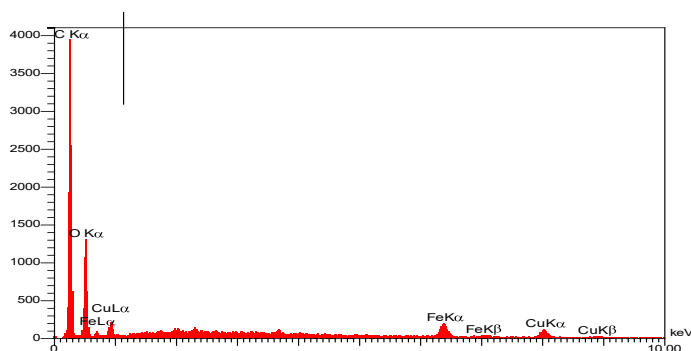Fig. 2: SEM images of G-Fe/Cu-NPs.

Fig. 3: EDX of prepared G-Fe/Cu-NPs sample.

strated in the results for three ratios in Fig. 5, a substantial increase in OG degradation was observed in the first 20 minutes due to the availability of active sites on the adsorbent surface that absorbed a high quantity of dye, but the rate of degradation slowed as unoccupied sites became saturated.

Effect of the Amount of G-Fe/Cu-NPs Dose

The impact of G-Fe/Cu-NPs dose on the degradation of OG was investigated. The dosage of nanoparticles was changed in the range 0.5-2.0 $g.L^{-1}$ by keeping the rest of the operating conditions constant (Fig. 6). The removal rate of OG were 10, 15, 19, 20, and 21 % for doses 0.5, 0.75, 1.0, 1.5, and 2.0 $g.L^{-1}$ respectively at 120 min period time. The removal effectiveness of OG improved as the number of G Fe/Cu-NPs was increased, owing to the availability of more vacant adsorption sites as the overall surface area of the adsorbate increased. Also, because of the repulsive forces that exist between the dyed surface and the adsorbate, the removal of OG increased dramatically at the start of contact time and then increased at a slow rate after reaching equilibrium, because it would be difficult to adsorbed OG ions by the remaining active sites (Mahmoud et al. 2019). However, as improving the removal of OG with more concentrated G-Fe/Cu-NPs, 1.0 $g.L^{-1}$ was chosen to be the optimum dose for
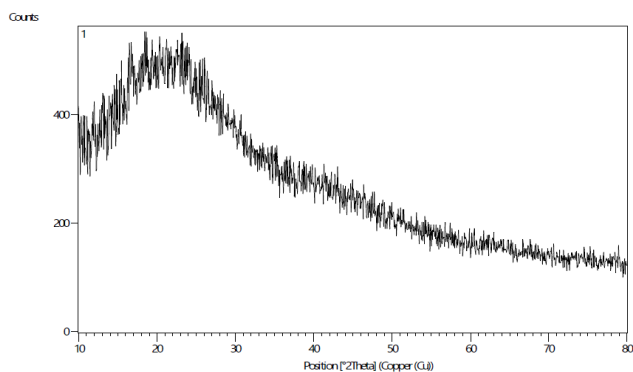
G-Fe/Cu-NPs among doses 1.5 and 2.0 g/L, due to nearest removal efficiency and because 1.0 $g.L^{-1}$ is cost-effective.

Effect of Initial pH

The surface of the adsorbent charge and the solubility qualities of adsorbate are organized by how acidic, neutral, or basic the working solution is, and this has a big impact on dye removal. Fig. 7 shows the OG removal efficiency at various pH 2, 3, 4, 5, 7, and 9 along with 120 min, whereas the other parameters were kept constant. The OG removal efficiencies were 12, 15, 19, 22, 24, and 20 respectively. The adsorption capacity of OG increases with acidic pH (2-6) until it reaches a maximum for G-Fe/Cu-NPs adsorbent at neutral pH7, after which it decreases as pH7 is exceeded. The dissociation of surface functional groups on G-Fe/Cu-NPs is the cause of this pH effect. As a result, pH7 is the best pH for removing OG.

Effect of Initial Concentration

Because the degradation rate is a function of the dye's starting concentration, it's an important metric to consider for successful adsorption. The initial concentration acts as a driving force, allowing dye ions to transfer between the liquid and solid phases despite their resistance. As a result, many OG concentrations of 10, 20, 30, 40, and 50 $mg.L^{-1}$ were tested to see how they affected the removal efficiency. The removal rates were 54%, 48%, 38%, 32%, and 24% respectively, under the other operation conditions. The degradation of OG declines with increasing dye concentrations, as shown in Fig. 8, indicating that unoccupied sites are available with

Fig. 4: XRD of prepared G-Fe/Cu-NPs sample.

Table 3: The BET parameters for G-Fe/Cu-NPs.

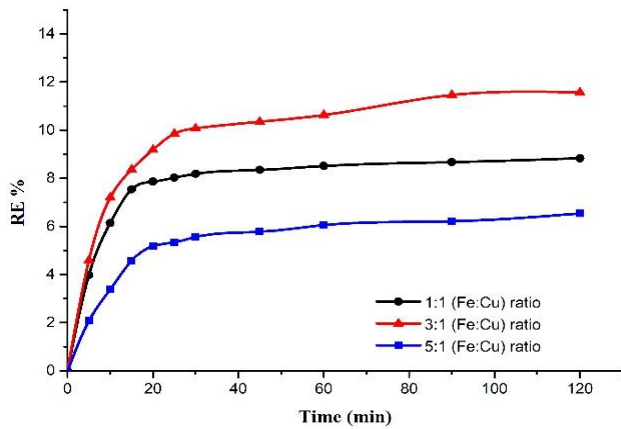| Parameter	Value
BET ($m^2.g^{-1}$)	3.243
Pore size (nm)	8.828
Pore volume ($cm^3.g^{-1}$)	0.016

Fig. 5: The OG Removal for the ratios of Fe to Cu (1:1, 3:1, and 5:1) at G-Fe/Cu-NPs dose, pH, initial concentration, temperature, agitation speed, and time were 0.5 g.L^{-1}, 4, 50 mg.L^{-1}, 25 °C, 150 rpm, and 120 min.
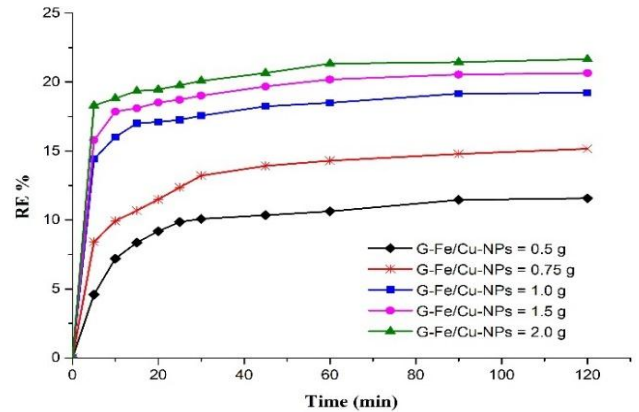

Fig. 6: Effect of the amount of G-Fe/Cu-NPs at initial OG concentration, pH, temperature, and agitation rate were 50 mg.L^{-1}, 4, 30 °C, and 150 rpm.

low OG concentrations, resulting in more dye ions moving toward these vacant sites of the nanoparticles. With increasing concentrations of OG, the adsorbent's available active sites decrease, resulting in a lower OG removal percentage.

Effect of Temperature

By keeping all the other operation conditions constant, the experiments with various temperatures of 30, 40, and 50 °C were carried out to examine the removal of OG with two initial concentrations of 10 and 50 mg.L^{-1}, as shown in Fig. 9. The removal percentages with 10 mg.L^{-1} of initial dye

concentration for the studied above temperatures were 54%, 47%, and 33% respectively, whereas the removal percentages for 50 mg.L^{-1} of initial concentration were 23%, 21%, and 10% respectively. It can be noted that the removal rate efficiency decreased with increasing the temperature from 30°C to 50°C, which means the adsorption of OG on G-Fe/Cu-NPs is exothermic in nature. The reason for decreasing removal efficiency with increasing temperature is probably due to the weakness of the adsorptive powers between the molecules of the adsorbed phases and also between the OG molecules and G-Fe/Cu-NPs active sites.

Table 4: Kinetic equations.

Model	Equation	Parameters
Pseudo-first order	$$\log(q_e - q_t) = \log q_e - \frac{k_1 t}{2.303}$$	q_t: adsorption capacities at time t (mg.g^{-1}). k_1: pseudo-first-order rate constant (min^{-1}).
Pseudo-second-order	$$\frac{t}{q_t} = \frac{1}{k_2 q_e^2} + \frac{t}{q_e}$$	k_2: pseudo-second order constant (g.[mg. min]$^{-1}$)
Elovich	$$q_t = \frac{1}{\beta} ln(\alpha\beta) + \frac{1}{\beta} ln(t)$$	α: initial adsorption rate constant (mg.[g .min]$^{-1}$) β: desorption rate constant (g.mg^{-1})

Table 5: The kinetic parameters for the adsorption of OG onto G-Fe/Cu-NPs at various initial dye concentrations.

OG (mg.L^{-1})	Pseudo-first order		Pseudo-second order		Elovich – Model		
	k_1	R^2	k_2	R^2	A	β	R^2
10	0.634	0.83	0.061	0.999	3.085	0.981	0.862
20	0.945	0.73	0.05	0.999	7.428	0.526	0.804
30	1.522	0.833	0.024	0.998	5.947	0.415	0.864
40	1.566	0.84	0.023	0.998	7.876	0.412	0.849
50	1.565	0.812	0.023	0.998	6.192	0.41	0.866

Effect of Agitation Intensity

The effect of agitation was investigated at speeds of 100, 150, 250, 400, and 600 rpm to see how much OG was removed at each of these rates. The batch adsorption studies were carried out at 1.0 g, 7, 10 mg.L^{-1}, and 30°C, with the dose of G-Fe/Cu-NPs, pH, and initial OG concentration set at 1.0 g, 7, 10 mg.L^{-1}, and 30°C, respectively. The results showed that mixing rates had no significant effect on OG degradation percentages. The phenomena can be shown by the controlling of adsorption rate, which was either by diffusion of film or pore, where at lower mixing speeds, the fluid film around the particle is thick and the rate-limiting step is perhaps diffusion of film. At greater mixing speeds, pore diffusion may be the rate-limiting stage since film diffusion has reached its maximum value. The fact that the resistance of the boundary layer is extremely tiny and the mobility of the process is highly regulated by the experimental conditions explains why varied agitation speeds are ineffective in this case. Alternatively, the ions of OG are diffused from the solution to the surface of G Fe/Cu-NPs and subsequently into the pores easily and quickly.

Adsorption Kinetics

The pseudo-first-order, pseudo-second-order, and Elovich models were used to estimate the adsorption data in the kinetic investigation (Ma et al. 2020)

To investigate the above kinetics, Table 4 shows the kinetic equations were used:

The value of constant rate k_1 can be found from the slope of the graph between $log\ (q_e - q_t)$ and time (t) as shown in Fig. 11-a. On the other hand, the values of k_2 and q_e for pseudo-second-order can be obtained from the slope and
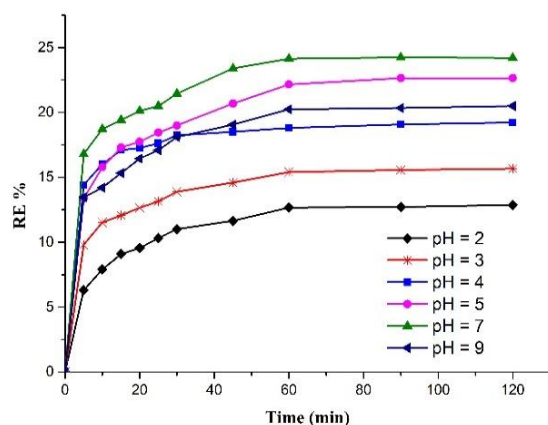
intercept of the plot between t/q_t versus t which is depicted in Fig. 11-b. It can be seen from Table 5 that the regression coefficient R^2 for pseudo-second-order is higher than R^2 for pseudo-first-order, which indicates that the pseudo-second-order kinetic model is the best fit model for OG kinetic adsorption by G-Fe/Cu-NPs.

The Elovich model is connected to the chemisorption kinetics of a solution onto the solid surface of adsorbents, as well as the activation energy and extent of surface coverage for chemisorption (Olivia et al. 2021). The values of Elovich coefficients α and β can be attained from the slope and intercept between q_t and ln (t) as presented in Fig. 11-c. It can be seen from Table 6 that the values of α and β are influenced by varying the initial concentration of OG, thus, as the initial OG concentration increased from 10-50 mg.L^{-1} the value of β decreased, and no significant variation with α. Also, the results illustrated that the rate of adsorption α is higher than desorption constant β, which indicated the viability of adsorption. Further, the value of the regression coefficient R^2 of the Elovich model was already low which referred to a poor fit for this model.

In conclusion from Table 5, it can be observed that the pseudo-second-order model was most suitable to represent the G-Fe/Cu-NPs system kinetics.

Adsorption Isotherm

The adsorption isotherm is commonly used to determine adsorbates and adsorbents' maximal sorption capacity. The Langmuir, Temkin, Freundlich, and Dubinin isotherm models are used to examine the interaction between G-Fe/Cu-NPs (the adsorbent) and OG (the adsorbed dye), and the formulae for these expressions are shown in Table 6.
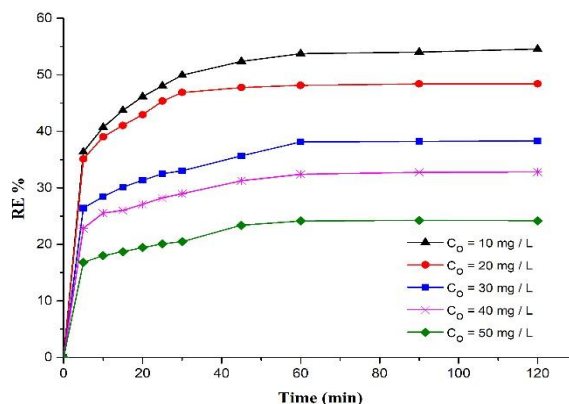

Fig. 7: Effect of initial pH at G-Fe/Cu-NPs dose, initial OG concentration, temperature, and agitation speed were 1 g.L^{-1}, 50 mg.L^{-1} OG, 30 °C, and 150 rpm.

Fig. 8: Effect of initial OG concentration at a dosage of G-Fe/Cu-NPs, pH, temperature, time, and agitation rate were 1 g.L^{-1}, 7, 30°C, 120 min, and 150 rpm.

The Langmuir parameters of q_{max} and K_L can be calculated from the slope and intercept of plot $1/q_e$ versus $1/C_e$. Furthermore, the separation factor R_L is a dimensionless constant which represents a good indicator of the Langmuir isotherm, this expression can be obtained by the equation:

$$R_L = \frac{1}{1 + K_L C_o}$$ ...(3)

Where R_L values was used to describe whether the adsorption is favorable when $R_L < 1$, linear when $R_L = 1$, unfavorable when $R_L > 1$, or irreversible when $R_L = 0$ (Al-Qahtani 2017).

Furthermore, the $1/n$ and K_F parameters of Freundlich isotherm can be found from the slope and intercept of graph Log C_e versus log K_F. In addition, the values of 1/n can verify if the isotherm is favorable when $0 < 1/n < 1$, unfavorable when $1/n > 1$ or irreversible when $1/n = 0$. The adsorption isotherm parameters are listed in Table 7, and Fig. 12 shows the isotherm models.

The data of isotherms in Table 7 indicated the Langmuir model has a good regression coefficient ($R^2 = 0.969$) and the values of R_L are ranged ($0 < R_L 1<$). These two parameters revealed a high degree of contact between the adsorbent and the adsorbate, as well as a favorable isotherm. Another indicator from the Freundlich isotherm is the value of the Freundlich constant KF, which indicates increased adsorption capacity because its value is substantial (2.43); also, the value

of 1/n is between 0 and 1, indicating a favorable isotherm. The maximum binding heat of sorption B_T obtained from Temkin isotherm was a positive number (0.263 kJ.mol^{-1}) and this refers to an exothermic adsorption process. The good regression coefficient R^2 obtained from Dubinin isotherm is higher also ($R^2 = 0.986$) which refers to the strong interaction between the reactive group of OG and the adsorbent G-Fe/Cu-NPs, further, the E value was (0.395 kJ.mol^{-1}) which indicated to the type of adsorption, this value referred to physisorption (Maguana et al. 2020). Finally, the Langmuir and Dubinin isotherms are the best fitting models for the adsorption of OG on the G-Fe/Cu-NPs.

Adsorption Thermodynamic

The OG adsorption onto bimetallic G-Fe/Cu-NPs was investigated at various temperatures (303, 313, and 323 K) to determine the adsorption spontaneity, adsorption nature, and adsorbent applicability. These properties of adsorption can be found from the thermodynamic parameters of standard Gibbs free energy ($\Delta G°$), standard enthalpy ($\Delta H°$), and standard entropy ($\Delta S°$) of the adsorption which derived by the following equations (Edet & Ifelebuegu 2020).

$$\Delta G° = \Delta H° - T \, \Delta S°$$ ...(4)

$$\Delta G° = -RT \, lnK_C$$ ...(5)

$$K_C = \frac{q_e}{C_e}$$ ...(6)

Table 6: Isotherm equations.

| Model	Equation	Parameters
Langmuir	$$\frac{1}{q_e} = \frac{1}{q_{max}.K_L}\left(\frac{1}{C_e}\right) + \frac{1}{q_{max}}$$	q_{max}: saturation adsorption of Langmuir (mg.L^{-1}). K_L: equilibrium constant of Langmuir (L.mg^{-1})
Freundlich	$$\log q_e = \left(\frac{1}{n}\right)\log C_e + \log K_F$$	K_F: the Freunlich adsorption constants. $1/n$: factor of heterogeneity
Temkin	$$q_e = B_T \, lnC_e + B_T \, lnK_T$$ $$B_T = \frac{RT}{b_T}$$	K_T: factor of the maximum binding energy (L.g^{-1}) B_T: maximum binding heat of sorption (KJ.mol^{-1}). R: ideal gas constant (0.008314 kJ.mol^{-1}.K^{-1}). T: absolute temperature (K).
Dubinin	$$nq_e = lnq_m - \beta\varepsilon^2$$ $$\varepsilon = RT \, ln\left(1 + \frac{1}{C_e}\right)$$ $$E = \frac{1}{\sqrt{(2\beta)}}$$	q_m: the theoretical saturation capacity β: Dubinin constant (mol^2.kJ^{-2}) ε: Dubinin isotherm constant E: adsorption energy (kJ.mol^{-1}).
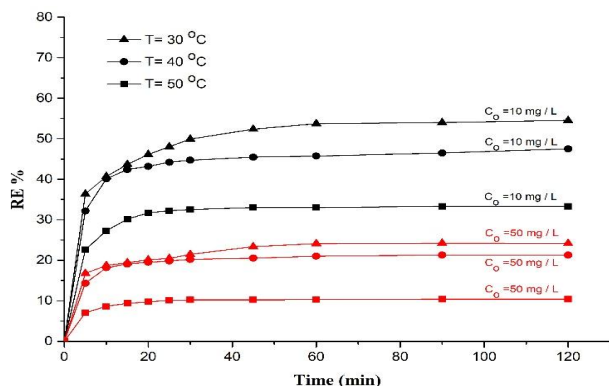
Fig. 9: Effect of temperature for 10 and 50 mg/L OG concentration, and at a dosage of G-Fe/Cu-NPs, pH, time, and agitation rate were 1 g.L^{-1}, 7, 120 min, and 150 rpm.
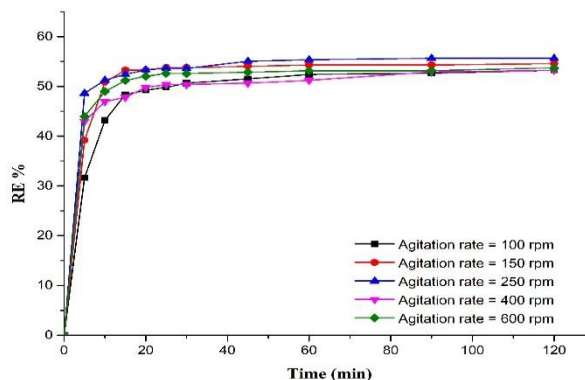

Fig. 10: Effect of agitation rate.

Where K_C is the distribution constant (L.g^{-1}). Hence, $\Delta S°$ and $\Delta H°$ can be obtained from the intercept and slope of graph $\Delta G°$ versus Temperature (K) as depicted in Fig. 13a.

Furthermore, the activation energy can be obtained from the Arrhenius equation shown below

$$lnk_{obs} = lnA - \frac{E_a}{RT} \qquad ...(7)$$

$$ln\left(\frac{C_t}{C_o}\right) = -k_{obs}\, t \qquad ...(8)$$

Where k_{obs} is the rate constant (min^{-1}), Ea is the activation energy (kJ.mol^{-1}), and A is the Arrhenius constant (J.mol^{-1}.K^{-1}). Ea represents the slope of the plot between ln (k_{obs}) versus 1/T as shown in Fig. 13b.

The thermodynamic parameters of OG adsorption onto G-Fe/Cu-NPs are illustrated in Table 8.

The Gibbs free energy $\Delta G°$ had a negative value at the optimum temperature studied (Table 8), thus confirming the spontaneity adsorption nature. On the other hand, the value of $\Delta G°$ (-0.462 kJ/mol) was between 0 kJ.mol^{-1} and -20 kJ.mol^{-1} which suggests a physisorption process (Romdhane et al. 2020). The negative value obtained for $\Delta H°$(-35.884 kJ.mol^{-1}) indicated that adsorption of OG onto G-Fe/Cu-NPs was an exothermic process of the adsorption process at the solid-solution interface and a suitable affinity of OG ions towards nanoparticles. The result of ($\Delta S°$) was positive (0.116 kJ.mol^{-1}.K^{-1}), indicating increased random interference of the adsorption process at the solid-liquid interface and an appropriate affinity of OG ions for nanoparticles (Edet & Ifelebuegu 2020).

Table 7: The isotherm parameters for the adsorption of OG onto G-Fe/Cu-NPs at various initial concentrations of OG.

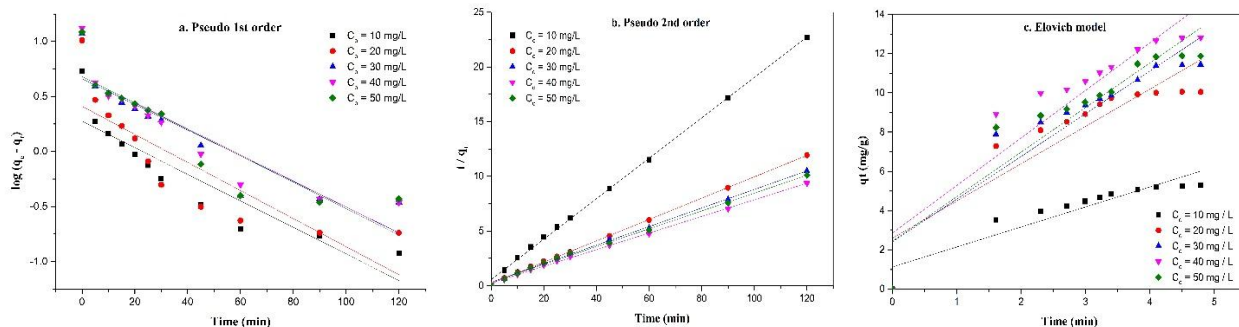| Langmuir				Freundlich			Temkin			Dubinin			
q_{max}	K_L	R^2	R$_L$	K_F	1/n	R^2	K_T	B_T	R^2	q_m	β	E	R^2
17.03	0.105	0.969	0.281	2.43	0.385	0.862	1	0.263	0.858	12.299	3.205	0.395	0.986

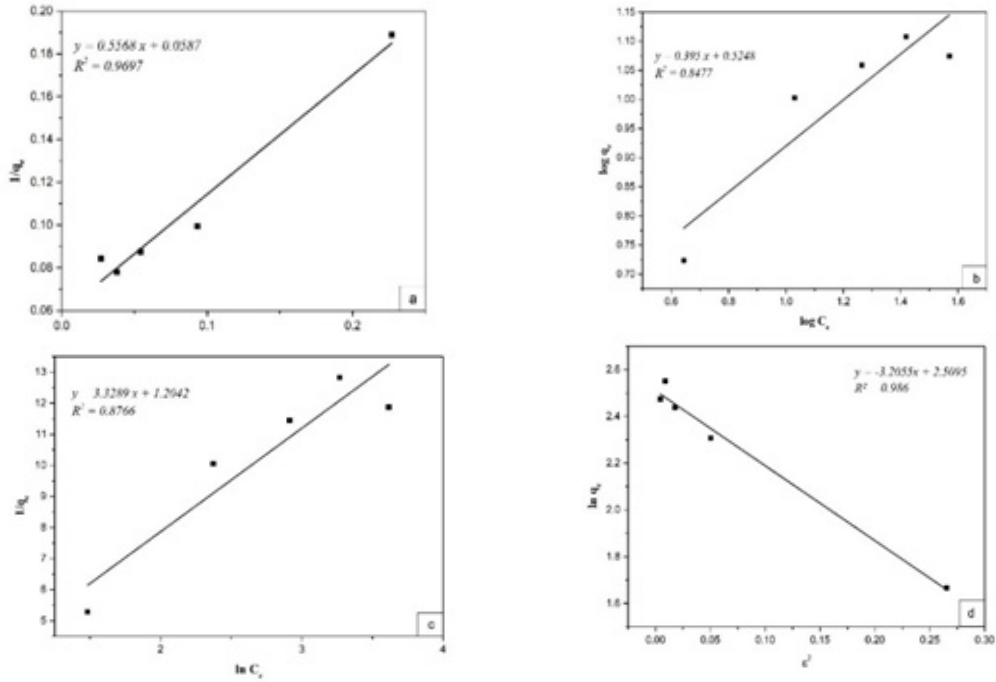Fig. 11: Kinetic models at a different initial concentration of OG adsorption.

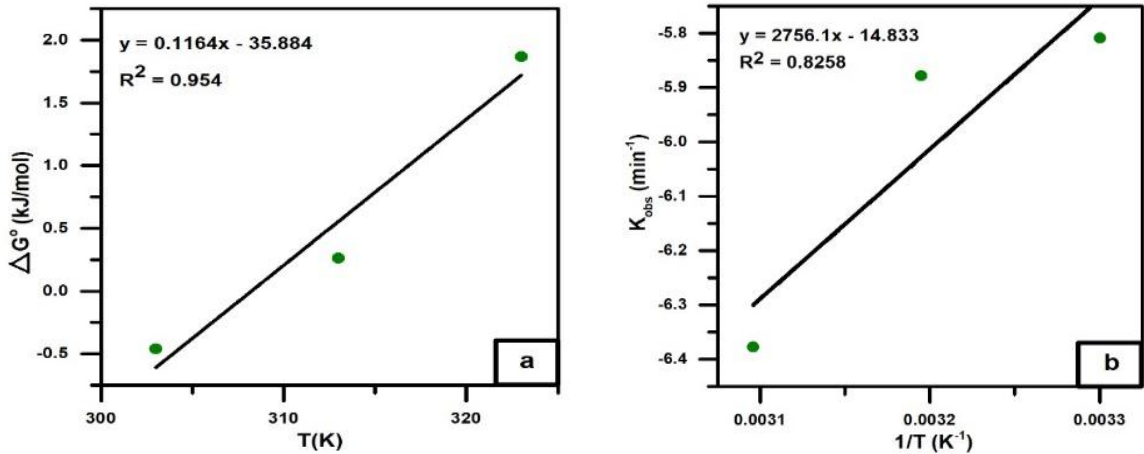Fig. 12: Isotherm models plots (a) Langmuir, (b) Freundlich, (C) Temkin, and (d) Dubnin isotherm.

Fig. 13: Thermodynamic parameters.

CONCLUSIONS

The effectiveness of the produced nanoparticles in relation to orange G dye adsorption in a batch system was tested in this work, which investigated a green preparation of bimetallic nanoparticles utilizing cost-effective material. Because of its availability and low cost, ficus extract has been demonstrated to be a viable material for capping and reducing agents. This study looked at the biosynthesis of bimetallic iron/copper

Table 8: Thermodynamic parameters.

Parameter	Value
$\Delta G°$ (kJ.mol^{-1})	-0.462
$\Delta H°$ (kJ.mol^{-1})	-35.884
$\Delta S°$ (kJ.mol.K^{-1})	0.116
E_a (kJ.mol^{-1})	-22.91
A	3.615×10^{-7}

nanoparticles with various ratios, and the optimal ratio of Fe to Cu for removing orange G dye was 3:1. However, this ratio was characterized using SEM, EDAX, XRD, and BET. Specifically, the semi-spherical and porous morphology of G-Fe/Cu-NPs was found with the diameter ranges from 32-59 nm and the surface area was 3.243 $m^2.g^{-1}$. In addition, the EDAX confirmed the bimetallic nature of nanoparticles by confirming the presence of iron and copper in the analyzed sample, while the amorphous of nanoparticles was confirmed by the XRD analysis. Then, using a comprehensive batch procedure, the adsorbent was tuned for all essential parameters. As a result, the G-Fe/Cu-NPs have a beneficial effect when used as adsorbents to remove OG, with batch trials yielding a final OG removal effectiveness of (54%) at the optimum conditions. It is found that the best values of the adsorption parameters such as G-Fe/Cu-NPs dose, pH, initial OG concentration, and temperature were 1 $g.L^{-1}$, 7, 10 $mg.L^{-1}$, and 30 respectively along with 120 min contact time, while the agitation speed showed no significant effect upon the degradation rate of OG.

The kinetic study exhibited that the removal of OG by G-Fe/Cu-NPs fit the pseudo-second-order kinetic model. Furthermore, the intra-particle diffusion of the adsorption mechanism demonstrated that the diffusion of OG inside the pore of G Fe/Cu-NPs is the rate-limiting step. Furthermore, the Langmuir and Dubinin isotherms were shown to be the most fitting models for the adsorption of OG on G Fe/Cu NPs. Furthermore, the Temkin model's binding heat of sorption was positive, indicating an exothermic adsorption process, and the adsorption energy showed physisorption adsorption. Finally, the adsorption thermodynamic parameters revealed the nature of spontaneity adsorption, physisorption, exothermic process, and random interference of the adsorption process, which increased at the solid-solution interface and a reasonable affinity of OG ions towards nanoparticles.

REFERENCES

Atiya, M., Ridha, M.J. and Saheb, M. 2020. Removal of aniline blue from textile wastewater using electrocoagulation with the application of the response surface approach. Iraqi J. Sci., 61: 114 doi: 10.24996/ijs.2020.61.11.4.

Abd El-Aziz, H.M., Farag, R.S. and Abdel-Gawad, S.A. 2020. Removal of contaminant metformin from water by using Ficus Benjamina zero-valent iron/copper nanoparticles. Nanotechnol. Environ. Eng., 5(3): 1-9. doi: 10.1007/s41204-020-00086-w.

Abdel-Aziz, H.M., Farag, R.S. and Abdel-Gawad, S.A. 2019. Carbamazepine removal from aqueous solution by green synthesis. Int. J. Environ. Res., 19: 220. doi: 10.1007/s41742-019-00220-w.

Al-Qahtani, K.M. 2017 Cadmium removal from aqueous solution by green synthesis zero-valent silver nanoparticles with Benjamina leaves extract. J. Aquat. Res., 43(4): 269-274. doi: 10.1016/j.ejar.2017.10.003.

Campos, S., Salazar, R., Arancibia-Miranda, N., Rubio, M.A., Aranda, M., García, A., Sepúlveda, P. and Espinoza, L.C. 2019. Nafcillin degradation by heterogeneous electro-Fenton process using Fe, Cu and Fe/Cu nanoparticles Sebastian. Chemosphere, 12: 813. doi: 10.1016/j.chemosphere.2020.125813.

Dhruval, S.R., Pai, N., Dhanwant, S.S., Hussein, B., Nayak, S., Rao, C.V., Kumar, A. and Janakaraj, M. 2020. Rapid synthesis of antimicrobial Fe/Cu alloy nanoparticles using waste silkworm cocoon extracts for cement mortar applications. Adv. Nat. Sc.: Nanosci. Nanotechnol., 11(2): 25006. doi: 10.1088/2043-6254/ab8790.

Edet, U.A. and Ifelebuegu, A.O. 2020. Kinetics, isotherms, and thermodynamic modeling of the adsorption of phosphates from model wastewater using recycled brick waste. Processes, 8(6): 665. doi: 10.3390/pr8060665.

Elahimehr, Z., Nemati, F. and Elhampour, A. 2020. Synthesis of a magnetic-based yolk-shell nano-reactor: A new class of monofunctional catalyst by Cu0-nanoparticles and its application as a highly effective and green catalyst for A3 coupling reaction effective and green catalyst for the A3 coupling reaction. Arab. J. Chem., 11: 211. doi: 10.1016/j.arabjc.2018.11.011.

Gopal, G., Sankar, H., Natarajan, C. and Mukherjee, A. 2020. Tetracycline removal using green synthesized bimetallic nZVI-Cu and bentonite supported green nZVI-Cu nanocomposite: A comparative study. J. Environ. Manag., 254: 109812. doi: 10.1016/j.jenvman.2019.109812.

Homaeigohar, S. 2020. The nanosized dye adsorbents for water treatment, Nanomaterials, 10(2): 295. doi: 10.3390/nano10020295.

Ismail, M., Khan, M., Khan, M.A. and Asiri, A.M. 2019. Pollution, toxicity, and carcinogenicity of organic dyes and their catalytic bio- remediation. Curr. Pharma. Design, 25(34): 3645-3663. https://doi.org/10.2174/1381612825666191021142026

Ma, P., Liu, Q., Liu, P., Li, H., Han, H., Liu, L. and Zou, W. 2020. Green synthesis of Fe/Cu oxides composite particles stabilized by pine needle extract and investigation of their adsorption activity for norfloxacin and ofloxacin. J. Dispers. Sci. Technol., doi: 10.1080/01932691.2020.1764367.

Maguana, Y., El, N., Elhadiri, M.B. and Chikri, R. 2020. Activated carbon for dyes removal: Modeling and understanding the adsorption process. J. Chem., 15: 683. doi: 10.1155/2020/2096834.

Mahmoud, A.S., Ismail, A., Mostafa, M.K., Mahmoud, M.S., Ali, W. and Shawky, A.M. 2019. Isotherm and kinetic studies for heptachlor removal from aqueous solution using Fe/ Cu nanoparticles, artificial intelligence, and regression analysis. Sep. Sci. Technol., 55(4): 684-696. doi: 10.1080/01496395.2019.1574832.

Olivia, E.N., Adimchinobi, E.S. and Uzoma, O.T. 2021. Equilibrium and kinetic studies of liquid-phase adsorption of methylene blue onto phosphoric acid modified Bambara nutshell. Acta Chem. Malay., 16: 222. doi: 10.2478/acmy-2021-0007.

Pavithran, S., Pappuswamy, M., Annadurai, Y., Arumugam, V.A. and Periyaswamy, T. 2020. Green synthesis of copper nanoparticles: Characterization and their application. J. Appl. Life Sci. Int., 23: 172. doi: 10.9734/JALSI/2020/v23i730172.

Romdhane, D.F., Satlaoui, Y., Nasraoui, R., Charef, A. and Azouzi, R. 2020. Adsorption, modeling, thermodynamic, and kinetic studies of methyl red removal from textile-polluted water using natural and purified organic matter-rich clays as low-cost adsorbent Dalila. J. Chem., 20: 617.

Tara, N., Siddiqui, S.I., Rathi, G., Chaudhry, S.A., Inamuddin, R. and Asiri, A M. 2019. Nano-engineered adsorbent for the removal of dyes from water: Rev. Curr. Anal. Chem., 16(1): 14-40. doi: 10.2174/1573411015666190117124344.

Wang, X., Jiang, C., Hou, B., Wang, Y., Hao, C. and Wu, J. 2018. Carbon composite lignin-based adsorbents for the adsorption of dyes, Chemosphere, 4: 183. doi: 10.1016/j.chemosphere.2018.04.183.